DYNAMIC RESPONSE OF ANISOTROPIC COMPOSITE PANELS TO TIME-DEPENDENT EXTERNAL EXCITATIONS

L. Librescu* and A. Nosier†
Department of Engineering Science and Mechanics
Virginia Polytechnic Institute and State University
Blacksburg, VA, 24061-0219, U.S.A.

Abstract

This paper deals with the dynamic response of anisotropic laminated composite flat panels exposed to sonic boom and explosive blast-type loadings.

The pertinent governing equations incorporating transverse shear deformation, transverse normal stress, the higher order effects as well as the viscous structural damping are solved by using the integral-transform technique. The obtained results are compared with their counterparts obtained within the framework of the first order transverse shear deformation and the classical plate theories and some conclusions concerning their range of applicability are outlined.

The paper also contains a detailed analysis of the influence played by the various parameters characterizing the considered pressure pulses as well as the material and geometry of the plate.

Introduction

The response of elastic structures to time-dependent external excitations, such as sonic boom and blast-type loadings, constitutes a subject which is currently of much interest in the design of aeronautical and space vehicles as well as of marine and terrestrial ones. With very few exceptions, its study was done in the past for the case of thin isotropic structural members (see e.g. [1-8]).

With the advent of the new composite material structures and their increased use in the aerospace as well as in the other fields of the advanced technology, there is a need to reconsider the problem of structural response. This is due to the fact that the new composite material structures exhibit distinguishing features as compared to their metallic counterparts. While the former ones are characterized by a weak rigidity in transverse shear and by high degrees of orthotropy of the layer materials, the latter ones are constituted of isotropic materials and may be considered to exhibit an infinite rigidity in transverse shear. That is why, in order to get correct results for the response behavior of flat structures made of advanced composite materials, refined plate models have to be used. They should incorporate transverse shear deformation and transverse normal stress and should account for the higher-order effects. Since transverse shear properties and damping characteristics are primarily matrix dependent, they would certainly play an important role in the dynamic response of composite material structures.

The analytical studies devoted to the dynamic response of shear deformable laminated and single layered flat panels to blast loadings are very few. In this sense, the reader is referred to [9-11] and [12], respectively. Within this paper, the far field overpressure produced by an aircraft flying supersonically in the earth's atmosphere (referred to as the sonic-boom pressure pulse), or by any supersonic projectile, rocket or missile [13,14], as well as the one resulting from an explosive blast (see [3, 5-10] are considered to predict the panel response. The time-history of the sonic-boom is described as an N-shaped pulse, whose negative phase duration is included as a variable in the analysis. As concerns the explosive blast, its time-history is approximated both as an exponentially decaying pressure pulse, and, in an approximated way, by a triangular pulse. The results obtained within a higher-order plate theory (HSDT) are compared with their first order transverse shear deformation (FSDT) and classical (CLT) counterparts and some conclusions concerning their range of applicability are outlined. In addition, the obtained numerical results allow one to draw conclusions about the influence played by the various physical and geometrical parameters entering the problem. Having in view that the severity of the dynamic response can be conveniently measured in terms of the dynamic magnification factor (DMF), its variation for several pulse shapes is also displayed in the paper. This paper constitutes a synthesis of the results reported in [15,16].

Governing Equations

The response problem will be analyzed within the framework of a higher order bending theory of cross-ply symmetrically laminated composite plates. Previously formulated in [17,18], this theory exhibits all the advantages embodied in its FSDT counterpart both with regards to the number of involved unknown quantities and the order of the associated governing equations. However, in contrast to FSDT, the present theory is based on: i) a parabolic distribution of transverse shear stresses across the plate thickness (thus

*Professor

†Graduate Research Associate

avoiding the need for a shear correction factor) and ii) the elimination of the contradictory assumptions involving the simultaneous consideration of zero transverse normal stress σ_{33} and zero transverse normal strain e_{33}. Furthermore, the results predicted by HSDT will be compared with the ones obtained within the framework of FSDT and CLT. By adopting the assumptions formulated in [17] and by referring the points of the mid-plane of the laminated composite rectangular (axb) plate to a Cartesian system of coordinates x-y parallel at each point with the principal material directions, the governing equations (see [15-18]) may be reduced to:

$$
\begin{aligned}
&a_1 W_{,xxx} + a_2 W_{,xyy} + a_3 \psi_{x,xx} + a_4 \psi_{x,yy} \\
&+ a_5 \psi_{y,xy} + a_6 \psi_x + a_7 W_{,x} = a_8 \ddot{\psi}_x + a_9 \ddot{W}_{,x}, \\
&b_1 W_{,yyy} + b_2 W_{,yxx} + b_3 \psi_{y,yy} + b_4 \psi_{y,xx} \\
&+ b_5 \psi_{x,xy} + b_6 \psi_y + b_7 W_{,y} = b_8 \ddot{\psi}_y + b_9 \ddot{W}_{,y}, \\
&c_1 \psi_{x,x} + c_2 \psi_{y,y} + c_3 W_{,xx} + c_4 W_{,yy} \\
&+ c_5 P_z = c_6 \ddot{W} + C\dot{W}.
\end{aligned}
\tag{1}
$$

The FSDT counterparts of Eqs. (1) are given by (see [15-18]):

$$
\begin{aligned}
&a_3 \psi_{x,xx} + a_4 \psi_{x,yy} + a_5 \psi_{y,xy} \\
&+ a_6 \psi_x + a_7 W_{,x} = a_8 \ddot{\psi}_x, \\
&b_3 \psi_{y,yy} + b_4 \psi_{y,xx} + b_5 \psi_{x,yx} \\
&+ b_6 \psi_y + b_7 W_{,y} = b_8 \ddot{\psi}_y, \\
&c_1 \psi_{x,x} + c_2 \psi_{y,y} + c_3 w_{,xx} \\
&+ c_4 W_{,yy} + c_5 P_z = c_6 \ddot{W} + C\dot{W}, ,
\end{aligned}
\tag{2}
$$

where, in contrast to HSDT, the higher order effects as well as the contribution of σ_{33} are disregarded. The coefficients appearing in Eqs. (1) and (2), which are functions of stiffness quantities, are displayed in Appendix I. In particular, the coefficients c_3 and c_4 include the effect of the in-plane edge loads T_{11} and T_{22}, respectively, which, as will be shown later, play a substantial role in the response behavior. The structural response corresponding to CLT can be obtained as a special case of FSDT by considering the transverse shear moduli to be infinite quantities. For convenience, in Eqs. (1) and (2), the notations W, ψ_x, and ψ_y replace $v_3^{(0)}$, $v_1^{(1)}$, and $v_2^{(1)}$, respectively, originally introduced in [17,18]. As a result, W, ψ_x, and ψ_y denote the transverse deflection and rotations of normal lines to the mid-plane (about the y and x-axes, respectively) while C denotes the transverse viscous damping coefficient. The boundary conditions for a simply-supported rectangular axb) plate are [15-17]

$$
\begin{aligned}
&\psi_y = 0, \; W = 0, \text{ and } a_1 W_{,xx} + \\
&+ a_3 \psi_{x,x} = 0 \text{ at } x = 0, a, \\
&\text{and} \\
&\psi_x = 0, \; W = 0, \text{ and } b_1 W_{,yy} + \\
&+ b_3 \psi_{y,y} = 0 \text{ at } y = 0, b.
\end{aligned}
\tag{3}
$$

while the initial conditions are prescribed to be:

$$
\begin{aligned}
&\psi_x(x,y,0) = \tilde{\psi}_x(x,y), \; \psi_y(x,y,0) \equiv \tilde{\psi}_y(x,y), \\
&W(x,y,0) \equiv \tilde{W}(x,y), \\
&W_{,x}(x,y,0) \equiv \tilde{W}_x(x,y), \; W_{,y}(x,y,0) \equiv \tilde{W}_y(x,y), \\
&\dot{\psi}_x(x,y,0) \equiv \tilde{\dot{\psi}}_x(x,y,), \\
&\dot{\psi}_y(x,y,0) \equiv \tilde{\dot{\psi}}_y(x,y), \; \dot{W}(x,y,0) \equiv \tilde{\dot{W}}(x,y), \\
&\dot{W}_{,x}(x,y,0) \equiv \tilde{\dot{W}}_x(x,y), \\
&\dot{W}_{,y}(x,y,0) \equiv \tilde{\dot{W}}_y(x,y).
\end{aligned}
\tag{4}
$$

Here, the single and double over tildes denote prescribed quantities for the basic variables ψ_x, ψ_y, W as well as for $W_{,x}$ and $W_{,y}$ and their time derivatives, respectively, at $t = 0$.

As concerns the boundary conditions associated with FSDT, they can be found e.g. in [17]. For the sake of completeness, they are displayed here also:

$$
\begin{aligned}
&\psi_y = 0, \; W = 0, \text{ and } \psi_{x,x} = 0 \text{ at } x = 0,a \\
&\text{and} \\
&\psi_x = 0, \; W = 0, \text{ and } \psi_{y,y} = 0 \text{ at } y = 0, b.
\end{aligned}
\tag{5}
$$

Solution Procedure

The integral-transform technique will be used to solve the dynamic-response problem. To this end, Eqs. (1) and (2) are subjected to a Laplace transform with respect to the time variable and successively $(1)_1$, $(1)_2$ and $(1)_3$ to finite Fourier cosine-sine, sine-cosine, and sine-sine transforms, respectively. Appropriate use of initial and boundary conditions given by Eqs. (3) and (4) yields an algebraic system of equations expressed in the transformed space as:

$$\begin{bmatrix} (K_{11} + a_8 s^2) & K_{12} & (K_{13} + a_9\alpha_m s^2) \\ K_{21} & (K_{22} + b_8 s^2) & (K_{23} + b_9\beta_n s^2) \\ K_{31} & K_{32} & (K_{33} + c_6 s^2 + Cs) \end{bmatrix} \begin{Bmatrix} \bar{\psi}_x^{(cs)}(m,n,s) \\ \bar{\psi}_y^{(sc)}(m,n,s) \\ \bar{W}^{(ss)}(m,n,s) \end{Bmatrix} = \begin{Bmatrix} \bar{T}_1 \\ \bar{T}_2 \\ \bar{T}_3 \end{Bmatrix} \quad (6)$$

In Eqs. (6) the following notations have been used:

$$K_{11} = a_3\alpha_m^2 + a_4\beta_n^2 - a_6;\ K_{12} = a_5\alpha_m\beta_n,$$

$$K_{13} = a_1\alpha_m^3 + a_2\alpha_m\beta_n^2 - a_7\alpha_m;\ K_{21} = b_5\alpha_m\beta_n,$$

$$K_{22} = b_4\alpha_m^2 + b_3\beta_n^2 - b_6;$$

$$K_{23} = b_1\beta_n^3 + b_2\beta_n\alpha_m^2 - b_7\beta_n,$$

$$K_{31} = c_1\alpha_m;\ K_{32} = c_2\beta_n;\ K_{33} = c_3\alpha_m^2 + c_4\beta_n^2,$$

$$\bar{T}_1 = sM_{11}^{(cs)}(m,n) + M_{12}^{(cs)}(m,n),$$

$$\bar{T}_2 = sM_{21}^{(sc)}(m,n) + M_{22}^{(sc)}(m,n), \quad (7)$$

$$\bar{T}_3 = sM_{31}^{(ss)}(m,n) + M_{32}^{(ss)}(m,n) +$$

$$+ c_5\bar{p}_z^{(ss)}(m,n,s),$$

where

$$M_{11}^{(cs)} = a_8\tilde{\bar{\psi}}_x^{(cs)}(m,n) + a_9\tilde{\bar{W}}_x^{(cs)}(m,n),$$

$$M_{12}^{(cs)} = a_8\tilde{\bar{\psi}}_x^{(cs)}(m,n) + a_9\tilde{\bar{W}}_x^{(cs)}(m,n), \quad (8)$$

$$M_{21}^{(sc)} = b_8\tilde{\bar{\psi}}_y^{(sc)}(m,n) + b_9\tilde{\bar{W}}_y^{(sc)}(m,n),$$

$$M_{22}^{(sc)} = b_8\tilde{\bar{\psi}}_y^{(sc)}(m,n) + b_9\tilde{\bar{W}}_y^{(sc)}(m,n),$$

$$M_{31}^{(ss)} = c_6\tilde{\bar{W}}_x^{(ss)}(m,n),$$

$$M_{32}^{(ss)} = c_6\tilde{\bar{W}}_y^{(ss)}(m,n) + C\tilde{\bar{W}}^{(ss)}(m,n).$$

In addition, $\alpha_m = m\pi/a$ and $\beta_n \equiv n\pi/b$; m and n denote Fourier transform variables associated with x and y, respectively, while s denotes Laplace transform variable associated with the time variable t. A bar over a quantitity identifies its Laplace transform (that is $\mathcal{L}\{a(t)\} \equiv \bar{a}(s)$) while $(\cdot)^{(s)}$ and $(\cdot)^{(c)}$ denote finite sine and cosine Fourier transforms, respectively. It should be remarked that the right-hand side of Eqs. (6) contains the initial conditions as part of the forcing function.

Two different problems which nevertheless are interrelated could be analyzed when starting with the system of Eqs. (6). These are the dynamic response and its associated eigenfrequency problem. While for the former problem the right-hand side of Eqs. (6) is different from zero, for the latter one it should be considered zero. From the system of equations (6), a formal solution to the dynamic response in the transformed space could be written as:

$$\begin{Bmatrix} \bar{\psi}_x^{(cs)}(m,n,s) \\ \bar{\psi}_y^{(sc)}(m,n,s) \\ \bar{W}^{(ss)}(m,n,s) \end{Bmatrix} = \sum_{j=1}^{3} \frac{\bar{T}_j}{\bar{D}} \begin{Bmatrix} \bar{F}_{1j}(m,n,s) \\ \bar{F}_{2j}(m,n,s) \\ \bar{F}_{3j}(m,n,s) \end{Bmatrix} \quad (9)$$

where $\bar{D}$ and $\bar{F}_{ij}$ are defined by:

$$\bar{D} = \lambda_1 s^6 + \lambda_2 s^5 + \lambda_3 s^4 + \lambda_4 s^3 + \lambda_5 s^2 + \lambda_6 s + \lambda_7$$

$$\equiv \lambda_1(s - s_1)(s - s_1^*)(s - s_2) \quad (10)$$

$$(s - s_2^*)(s - s_3)(s - s_3^*),$$

and

$$\bar{F}_{ij}(m,n,s) = \sum_{r=1}^{5} I_{ijr} s^{5-r}. \quad (11)$$

The coefficients λ_i and I_{ijr} are displayed in the Appendix 1 of [16]. In Eq.(10), s_k ($k = \overline{1,3}$) and their complex conjugates s_k^* are assumed to be the six roots of $\bar{D} = 0$. Now by writing

$$s_k = -\beta_k + J\omega_k\ ,\ (J = \sqrt{-1})$$

Eq. (10) can alternatively be written in a more convenient form as:

$$\bar{D} = \lambda_1[(s + \beta_1)^2 + \omega_1^2][(s + \beta_2)^2 + \omega_2^2]$$
$$[(s + \beta_3)^2 + \omega_3^2]. \quad (12)$$

In order to obtain the response in the real time domain it is essential to determine:

$$\mathcal{L}^{-1}\{\bar{F}_{ij}/\bar{D}\} \equiv H_{ij}(m,n,t),$$

and

$$\mathcal{L}^{-1}\{s\bar{F}_{ij}/\bar{D}\} \equiv L_{ij}(m,n,t). \quad (13)$$

To this end, the partial fraction expansion is used to express $\bar{F}_{ij}/\Delta$ as:

$$\frac{\bar{F}_{ij}}{\Delta} = \sum_{k=1}^{3} \frac{A_{ijk}(s + \beta_k) + B_{ijk}\omega_k}{(s + \beta_k)^2 + \omega_k^2}, \tag{14}$$

where A_{ijk} and B_{ijk} are real coefficients (see Appendix 2 of [16]). Based on the representation (14), it may be shown that $H_{ij}(m,n,t)$ (playing the role of impulse response function) results in the form:

$$H_{ij}(m,n,t) = \sum_{k=1}^{3} e^{-\beta_k t}(A_{ijk}\cos\omega_k t + B_{ijk}\sin\omega_k t) \tag{15}$$

As concerns $L_{ij}(m,n,t)$, from $(13)_2$ we obtain

$$L_{ij}(m,n,t) = \int_0^t \dot{\delta}(t-\tau)H_{ij}(m,n,\tau)d\tau = \dot{H}_{ij}(m,n,t) + H_{ij}(m,n,0)\delta(t), \tag{16}$$

where $\delta \equiv \delta(t)$ denotes Dirac's distribution while τ is a dummy time variable.

However, by virtue of the relationship

$$H_{ij}(m,n,0) = \sum_{r=1}^{3} A_{ijk} = 0,$$

Eq. (16) reduces finally to the form:

$$L_{ij}(m,n,t) = \dot{H}_{ij}. \tag{17}$$

The inverse Laplace transform applied to Eqs. (9) yields the response quantities in the time domain as:

$$\begin{aligned}
\psi_x^{(cs)}(m,n,t) &= M_{11}^{(cs)}L_{11}(m,n,t) + M_{12}^{(cs)}H_{11}(m,n,t) \\
&+ M_{21}^{(sc)}L_{12}(m,n,t) + M_{22}^{(sc)}H_{12}(m,n,t) \\
&+ M_{31}^{(ss)}L_{13}(m,n,t) + M_{32}^{(ss)}H_{13}(m,n,t) \\
&+ \int_0^t H_{13}(m,n,t-\tau)\, P_z^{(ss)}(m,n,\tau)\, d\tau, \\
\psi_y^{(sc)}(m,n,t) &= M_{11}^{(cs)}L_{21}(m,n,t) + M_{12}^{(cs)}H_{21}(m,n,t) \\
&+ M_{21}^{(sc)}L_{22}(m,n,t) + M_{22}^{(sc)}H_{22}(m,n,t) \\
&+ M_{31}^{(ss)}L_{23}(m,n,t) + M_{32}^{(ss)}H_{23}(m,n,t) \\
&+ \int_0^t H_{23}(m,n,t-\tau)\, P_z^{(ss)}(m,n,\tau)\, d\tau, \\
W^{(ss)}(m,n,t) &= M_{11}^{(cs)}L_{31}(m,n,t) + M_{12}^{(cs)}H_{31}(m,n,t) \\
&+ M_{21}^{(sc)}L_{32}(m,n,t) + M_{22}^{(sc)}H_{32}(m,n,t) \\
&+ M_{31}^{(ss)}L_{33}(m,n,t) + M_{32}^{(ss)}H_{33}(m,n,t) \\
&+ \int_0^t H_{33}(m,n,t-\tau)\, P_z^{(ss)}(m,n,t)\, d\tau.
\end{aligned} \tag{18}$$

For zero initial conditions, the time-histories of the basic unknown functions (18) reduce in the Fourier space to:

$$\begin{aligned}
\psi_x^{(cs)}(m,n,t) &= \sum_{k=1}^{3} \int_0^t e^{-\beta_k\tau}(A_{13k}\cos\omega_k\tau + B_{13k}\sin\omega_k\tau)P_z^{(ss)}(t-\tau)d\tau, \\
\psi_y^{(sc)}(m,n,t) &= \sum_{k=1}^{3} \int_0^t e^{-\beta_k\tau}(A_{23k}\cos\omega_k\tau + B_{23k}\sin\omega_k\tau)P_z^{(ss)}(t-\tau)d\tau, \\
W^{(ss)}(m,n,t) &= \sum_{k=1}^{3} \int_0^t e^{-\beta_k\tau}(A_{33k}\cos\omega_k\tau + B_{33k}\sin\omega_k\tau)P_z^{(ss)}(t-\tau)d\tau.
\end{aligned} \tag{19}$$

In the following developments, for computational reasons, Eq. $(19)_3$ will be expressed in an equivalent form as:

$$W^{(ss)}(m,n,t) = \sum_{k=1}^{3} \int_0^t e^{-\beta_k(t-\tau)}(A_{33k}\cos\omega_k(t-\tau) + B_{33k}\sin\omega_k(t-\tau))P_z^{(ss)}(m,n,\tau)d\tau. \tag{20}$$

Successive application of inverse sine and cosine Fourier transforms to Eqs. (18) or (19) yields the primary response quantities in the physical space expressed as [15,16]:

$$\psi_x(x,y,t) = \frac{1}{a}\psi_x^{(c)}(0,y,t) + \frac{4}{ab}\sum_{m=1}^{\infty}\sum_{n=1}^{\infty}\psi_x^{(cs)}(m,n,t)\sin\beta_n y\cos\alpha_m x,$$

$$\psi_y(x,y,t) = \frac{2}{a}\sum_{m=1}^{\infty}[\frac{1}{b}\psi_y^{(sc)}(m,0,t)$$

$$+\frac{2}{b}\sum_{n=1}^{\infty}\psi_y^{(sc)}(m,n,t)\cos\beta_n y]\sin\alpha_m x,$$

$$W(x,y,t) = \frac{4}{ab}\sum_{m=1}^{\infty}\sum_{n=1}^{\infty}w^{(ss)}(m,n,t)\sin\beta_n y\ \sin\alpha_m x, \tag{21}$$

where

$$\psi_x^{(c)}(m,y,t) = \frac{2}{b}\sum_{n=1}^{\infty}\psi_x^{(cs)}(m,n,t)\ \sin\beta_n y.$$

Needless to say that the above equations could be applied to determine the structural response of viscously damped cross-ply symmetrically laminated plates to any time-dependent excitation. However, in the forthcoming developments the case of N-shaped pulse and blast-type loadings will be considered only. In addition, the solution given by Eqs. (18)-(21) is applicable also to the FSDT, in which case the proper coefficients a_i, b_i and c_i should be used.

It should be mentioned in passing that for the case $C \to 0$, the equations (15)-(20) reduce to their undamped counterparts as developed in [15].

Response to Blast and Sonic Boom-Type Loadings

Within the present paper, several results which concern the response of composite flat panels to explosive blast and sonic boom-type loadings, synthesizing the ones obtained in [15,16], will be presented. Due to their structural damaging effects, these types of loadings have been estimated by using both theoretical and experimental considerations. For the case of blast type loadings, various analytical expressions have been proposed and discussed in the literature (see e.g. [5,9 and 10]). As it was clearly established, the blast wave reaches the peak value in such a short time that the structure can be assumed to be loaded instantly. Due to the relative small dimensions of the plate when compared to the blast (and sonic boom) wave front, it may also be assumed that the pressure is uniformly distributed over the plate. The overpressure-time history can be described in terms of the modified Friedlander exponential decay equation [7,8]:

$$P_z(x,y,t)\ (\equiv P_z(t)) = P_m(1 - \frac{t}{t_p})\ e^{-a't/t_p}, \tag{22}$$

where the negative phase of the blast is included. In Eq. (22), P_m denotes the peak reflected pressure in excess of the ambient one; t_p denotes the positive phase duration of the pulse measured from the time of arrival of the blast at the plate surface; and a' denotes a decay parameter which has to be adjusted to approximate the pressure curve from the blast test. A depiction of the ratio P_z/P_m vs. time for various values of the ratio a'/t_p and a fixed value of t_p is displayed in Fig. 1. As it could be inferred, the triangular load may be viewed as a limiting case of (22), that is for $a'/t_p \to 0$.

As concerns the sonic boom loadings, they could be modelled as an N-shaped pressure pulse. Such a pulse corresponds to an idealized far field sonic boom disturbance arriving at a normal incidence. The pressure time-history of the N-wave shock pulse experienced by the plate may be described by [2-4,13,14]:

$$P_z(x,y,t)\ (\equiv P_z(t)) = \begin{cases} P_m(1 - \frac{t}{t_p}) & \text{for } 0 < t < rt_p \\ 0 & \text{for } t < 0 \text{ and } t > rt_p, \end{cases} \tag{23}$$

where r denotes the shock pulse length factor, and P_m and t_p maintain the same meaning as in the case of blast-type loadings. It may easily be seen that: i) for $r = 1$, the N-shaped pulse degenerates into a triangular one; ii) for $r = 2$, a symmetric N-shaped pressure pulse is obtained; while iii) for $1 < r < 2$, the N-shaped pulse becomes an asymmetric one as shown in Fig. 2. Another special case emerging from the N-shaped pulse occurs when $r = 1$ and $t_p \to \infty$, or from the blast pulse when $t_p \to \infty$. In this case the time duration of the pulse becomes infinite and consequently the pressure pulse becomes a step pulse.

In addition to the transverse deflection time-history, the dynamic magnification factor (DMF) of the transverse deflection produced by these pulses will also be determined.

As is well known, this factor is defined as the ratio of the largest (in the absolute sense) dynamic deflection to its static counterpart at a point on the structure.

Numerical Illustrations

Four types of structures will be considered in the subsequent numerical illustrations. The first one labelled "Structure A" is a three-layered cross ply (0°, 90°, 0°) square plate whose mid-layer is two times thicker than the external ones. Also it is assumed that the orthotropic material of all laminae is the same, being characterized by:

$$E_1 = 19.2 \times 10^6 \text{ psi}, E_2 = 1.56 \times 10^6 \text{ psi},$$

$$E_3 = 1.56 \times 10^6 \text{ psi},$$

$$G_{12} = 0.82 \times 10^6 \text{ psi}, G_{13} = 0.82 \times 10^6 \text{ psi},$$

$$G_{23} = 0.523 \times 10^6 \text{ psi},$$

$$\nu_{12} = \nu_{13} = 0.24, \nu_{23} = 0.49.$$

The second structure labelled "Structure B" is also a three-layered square plate, whose mid-layer is two times thicker than the external ones. It is assumed that the material of the laminae is transversely-isotropic, the plane of isotropy being parallel at each point to the mid-plane of the structure. It is further assumed that the material properties of the layers are:

$$E_{(2)} / G'_{(2)} = 20;\ E_{(1)}/G'_{(1)}\ (\equiv E_{(3)}/G'_{(3)}) = 50;$$

$$E_{(1)} / E'_{(1)}\ (\equiv E_{(3)}/E'_{(3)}) = 5;\ E_{(2)}/E'_{(2)} = 2;$$

$$E_{(1)} / E_{(2)} = E_{(3)} / E_{(2)} = 10;$$

$$\nu_{(i)} = \nu'_{(i)} = 0.24,\ (i = 1,2,3).$$

Here, the indices 1 and 3 are associated with the external layers while the index 2 with the mid-layer; E and ν are the Young's modulus and Poisson's ratio, respectively, associated with the isotropy plane; while E', ν' and G' denote the Young's modulus, Poisson's ratio and transverse shear modulus, respectively, in the planes normal to the isotropy plane. For both structures, the material density for all layers is taken as $\rho = 13 \times 10^{-5}$ lb sec^2/in^4.

The "Structure C" and "Structure D" are characterized by: Structure C: A three-layered (0°, 90°, 0°) square plate, while, Structure D: A nine-layered $(0°, 90°, 0°)_3$ square plate. In these cases it is assumed that the layers are of equal thickness and that they are constituted of the same orthotropic material defined by:

$$E_1 = 30 \times 10^6 \text{ psi},\ E_2 = E_3 = 0.75 \times 10^6 \text{ psi}$$

$$G_{12} = 0.45 \times 10^6 \text{ psi},\ G_{13} = 0.37 \times 10^6 \text{ psi},$$

$$G_{23} = G_{13}$$

$$\nu_{12} = \nu_{13} = \nu_{23} = 0.25$$

$$\rho = 0.000143 \text{ lb sec}^2/\text{in}^4$$

In addition, the numerical results will include the nondimensional viscous damping parameter defined by $\Delta/\pi(\equiv C/c_6\omega)$, where ω denotes the fundamental undamped eigenfrequency determined within CLT while $c_6 \equiv m_1$ stands for the mass term (see Appendix I).

Based on the previous theoretical results, Figs. 3 and 4 diplay the time-history of the dimensionless plate center deflection for the case of a blast loading; Fig. 5 and Figs. 6-9 depict the time-history of the nondimensional transverse deflection to a step and a N-pressure pulse, respectively. Figures 10 and 11 display the influence of in-plane tensile edge-loads and of transverse shear flexibility on the time-history response of a dimensionless transversely-single-layered plate to a step pulse of finite duration (t_p = 0.004 sec). In addition to these graphs, Figs. 12-14 display the variation of DMF to a N-pulse and blast-pulse, respectively, determined at the center of the plate vs. ωt_p, where ω is the fundamental undamped frequency determined within the HSDT.

Discussion and Conclusions

In Figs. 3 and 4, the dimensionless deflection V(≡ W/h) response of the center of a three-layered square plate to a normal blast loading is displayed. Figure 3 shows that with the decrease of the parameter a', higher amplitudes of the deflection are obtained. Figure 4 compares the deflection response obtained within HSDT, FSDT (with two shear correction factors) and CLT. As it results from these plots (obtained for the Structure B), k^2 = 2/3 gives better results when compared to their counterpart obtained with k^2 = 5/6. Opposite results are obtained when Structure D is considered. In this case, K^2 = 5/6 constitutes a better selection of the shear correction factor than K^2 = 2/3. This trend reveals once more the importance of approaching the response in the framework of a higher-order plate theory, which in contrast with FSDT does not require incorporation of such a correction factor, largely dependent on the lamination sequence, relative anisotropy of the layers, etc. The numerical results obtained for the response to a step pulse of infinite duration (see Fig. 5), reveal that the damping plays a great and constant role in reducting the deflection amplitudes.

Figures 6-9 display the deflection response of the center of a square plate to a sonic boom. While Fig. 6 reveals the quantitative and qualitative differences in the response deflections due to a symmetric (r = 2), asymmetric (r = 1.5) and a degenerated (r = 1) N-shaped pulse, Fig. 7 reveals the strong influence played by the parameter t_p (that is by the duration of the positive phase of N-shaped pulse). This figure also shows that even in the case of non-thick plates (that is when a/h = 20), the results obtained within the framework of the classical theory are in total disagreement with the ones incorporating transverse shear deformation effects. While during the positive phase of the pulse, the deflection response obtained as per the CLT follows the well known trend (in the sense that it is underestimated), within the negative phase of the pulse, it may result in higher values as compared to their shear deformable counterparts. However, for thin plates, the results (not displayed here), reveal that the response characteristics obtained within classical and shear deformable theories are in perfect agreement. Figures 7 through 9 reveal again the strong influence played by the parameter t_p principally within and after the negative phase of the pulse, as well as the unreliable character of the results furnished by the CLT.

In connection with the sonic boom pulse and the triangular one, two different regions of their response could be observed: a former one, occuring during the forced motion and a latter one, occuring during the free motion (that is after the wave has left the structure).

However, for the sonic boom-pulse two more distinguished regions could be discerned, namely, the ones associated with the positive

and negative pressure pulse. For the N-shape pulse (depending on the values of t_p and r), the largest (in the absolute sense) dynamic deflection can occur in these three regions appearing explicitly as three different branches of the DMF curves (as indicated in Figs. 12-14).

Figure 6 reveals that for the two pulse loadings characterized by r = 1 (triangular blast) and r = 2 (symmetrical sonic-boom) the response corresponding to the common time phase $0 < t < t_p$ is identical. However, for $t > t_p$ the time-histories produced by these two pulses are totally different. Another conclusion is that the two structures C and D yield, for the same pressure field, practically the same response behavior. Like Fig. 6, Fig. 13 reveals that during the free oscillation range (i.e., $t > rt_p$ (= 0.02 sec)), there are instances when CLT could result in higher deflection amplitudes than its HSDT counterpart.

The same conclusion emerges also from Figs. 12 and 13 where there are depicted the DMF curves against ωt_p, for an asymmetrical (r = 2.5) sonic boom pulse. As a general conclusion (obtained also in the case of metallic type structures [4-6]), the most significant amplitude attenuation due to the damping effect occurs during the free motion range (see Fig. 14) and 12, 13, and 15. However, Figs. 13 and 15 reveal that there are few instances during the free motion range when the damped oscillations exhibit higher deflection amplitudes than their undamped counterparts.

Figure 13 reveals that for r = 1.5, the negative phase of the pulse plays a reduced role in the amplitude magnification response, the main role being played by the positive phase. As it could be seen from the same figure, the branch of the DMF generated by the positive phase of the pulse coincides with the one generated by a triangular pulse (r = 1).

Figure 10 reveals the beneficial effect of in-plane tensile edge loads while Figure 11 shows the influence of transverse shear flexibility of the material of the plate on the dynamic response. Figure 11 reveals that the predictions of the classical theory are insensitive to any variation of transverse shear flexibility.

Finally, Figs. 7, 8, 11, and 13 as well as the previous ones, reveal that the assumption of the infinite rigidity in transverse shear as implied by the CLT provides unreliable results even for non-thick composite plates in the sense that the time-history deflection is generally underpredicted.

Based on these findings it may be concluded that a consistent evaluation of the time-history structural response of composite flat panels and implicitly, a rational design could be accomplished within a theory taking into account their flexibility in transverse shear.

It should also be added that in a number of cases the external excitations exhibit a random character and as a result, the response characteristics have to be determined in a probabilistic sense. For such a treatment of the problem where the response of composite laminated plates to random excitation was analyzed, see e.g. [19-21].

Acknowledgement

The partial support of this work by NASA Langley Research Center through Grant NAG-1-749 is gratefully acknowledged.

References

1. Crocker, M. J., Multimode Response of Panels to Normal and to Travelling Sonic Booms, J. Acoust. Soc. Am., 1967, 42, 1070.

2. Crocker, M. J., and Hudson, R. R., Structural Response to Sonic Booms, J. Sound Vibrations, 1969, 9 (3), pp. 454-468.

3. Crocker, M. J., Theoretical and Experimental Response of Panels to Travelling Sonic Boom and Blast Waves, Wyle Laboratories - Research Staff, Rept. WR 66-2, 1966.

4. Cheng, D. H. and Benveniste, J. E., Sonic Boom Effects on Structures - A Simplified Approach, Trans. N.Y. Acad. Sci., Ser. II 30, 457-478, 1968.

5. Houlston, R., Slater, J. E., Pegg, N. and Des Rochers, C. G., "On the Analysis of Structural Response of Ship Panels Subjected to Air Blast Loading." Comput. Struct. 21, pp. 273-289 (1985).

6. Rajamani, A. and Prabhakaran, R., "Response of Composite Plates to Blast Loading." Expl. Mech. 20, pp. 245-250. (1980).

7. Gupta, A. D., "Dynamic Analysis of a Flat Plate Subjected to an Explosive Blast." Proc. ASME Int. Computers Engineering Conf. 1, pp. 491-496 (1985).

8. Gupta, A. D., Gregory, F. H., and Bitting, R. L. "Dynamic Response of a Simply Supported Rectangular Plate to an Explosive Blast." Proc. XIII Southeastern Conf. on Theoretical and Appl. Mech. 1, pp. 385-390 (1985).

9. Dobyns, A. L., "Analysis of Simply-Supported Orthotropic Plates Subject to Static and Dynamic Loads. AIAA J. 19, pp. 642-650 (1981).

10. Birman, V., and Bert, C. W., "Behavior of Laminated Plates Subjected to Conventional Blast," Int. Journal of Impact Engng., vol. 6, No. 3, pp. 145-155, 1987.

11. Khdeir, A. A., and Reddy, J. N., "On the Forced Motions of Antisymmetric Cross-Ply Laminated Plates," Int. J. Mech. Sci., Vol. 31, No. 7, pp. 499-510, 1989.

12. Librescu, L., Khdeir, A. A., and Reddy, J. N., "Further Results Concerning the Dynamic Response of Elastic Orthotropic Plates," Z. Angew. Math. Mechanik 70, 1, pp. 23-33, 1990.

13. Gottlieb, J. J. and Ritzel, D. V., Analytical Study of Sonic Boom From Supersonic Projectiles, Progress in Aerospace Sciences, vol. 25, pp. 131-188, 1988.

14. Cheng, D. H., and Benveniste, J. E., "Transient Response of Structural Elements to Travelling Pressure Waves of Arbitrary Shape," Int. J. Mech. Sci., 8, 1966, pp. 607-618.

15. Librescu, L., and Nosier, A., "Response of Shear Deformable Elastic Laminated Composite Flat Panels to Sonic Boom and Explosive Blast Loadings," AIAA Journal, Vol. 28, 2, February 1990, pp. 345-352.

16. Nosier, A., Librescu, L., and Frederick, D., "The Effect of Time-Dependent Excitation on the Oscillatory Motion of Viscously Damped Laminated Composite Flat Panels," in "Advances in the Theory of Plates and Shells," Eds. G. Z. Voyiadjis and D. Karamanlides, Elsevier Science Publishers, B.V., Amsterdam, 1990, pp. 249-268.

17. Librescu, L., and Khdeir, A. A., "Analysis of Symmetric Cross-Ply Laminated Elastic Plates Using a Higher Order Theory," Part I, Composite Structures, 7, 1988, pp. 189-213.

18. Khdeir, A. A. and Librescu, L., "Analysis of Symmetric Cross-Ply Laminated Elastic Plates Using a Higher Order Theory," Part II, Composite Structures 9, 1988, pp. 259-277.

19. Cederbaum, G., Librescu, L., and Elishakoff, I., "Dynamic Response of Flat Panels Made of Advanced Composite Materials Subjected to Random Excitation," J. Acoust. Soc. Am., 84 (2), 1988, pp. 660-666.

20. Cederbaum, G., Elishakoff, I., and Librescu, L., "Random Vibrations of Laminated Plates Modeled Within the First-Order Shear Deformation Theory," Composite Structures, 12, 1989, pp. 97-111.

21. Cederbaum, G., Librescu, L., and Elishakoff, I., "Response of Laminated Plates to Non-Stationary Random Excitation," Structural Safety, 6, 1989, pp. 99-113.

Appendix I

The coefficients of Eqs. (1) are:

$$a_1 = -\frac{4}{3h^2} F_{11}^{11} - \delta_A\left(M_{11}^{11} - \frac{4}{3h^2} N_{11}^{11}\right),$$

$$a_2 = -\frac{4}{3h^2} \left(F_{22}^{11} + 2F_{12}^{12}\right) - \delta_A\left(M_{22}^{11} - \frac{4}{3h^2} N_{22}^{11}\right),$$

$$a_3 = D_{11}^{11} - \frac{4}{3h^2} F_{11}^{11} - \delta_A\left(M_{11}^{11} - \frac{4}{3h^2} N_{11}^{11}\right),$$

$$a_4 = D_{12}^{12} - \frac{4}{3h^2} F_{12}^{12},$$

$$a_5 = D_{22}^{11} - \frac{4}{3h^2} F_{22}^{11} + D_{12}^{12} - \frac{4}{3h^2} F_{12}^{12} - \delta_A\left(M_{22}^{11} - \frac{3}{3h^2} N_{22}^{11}\right),$$

$$a_6 = -R_{13}^{13} + \frac{4}{h^2} S_{13}^{13} = a_2,$$

$$a_8 = \delta_c\left(m_3 - \frac{4}{3h^2} m_5\right),$$

$$a_9 = -\delta_A\delta_B I_{33}^{11} - \delta_c \frac{4}{3h^2} m_5,$$

$$b_1 = -\frac{4}{3h^2} F_{22}^{22} - \delta_A\left(M_{22}^{22} - \frac{4}{3h^2} N_{22}^{22}\right),$$

$$b_2 = -\frac{4}{3h^2} \left(F_{11}^{22} + 2F_{21}^{21}\right) - \delta_A\left(M_{11}^{22} - \frac{4}{3h^2} N_{11}^{22}\right),$$

$$b_3 = D_{22}^{22} - \frac{4}{3h^2} F_{22}^{22} - \delta_A\left(M_{22}^{22} - \frac{4}{3h^2} N_{22}^{22}\right),$$

$$b_4 = D_{21}^{21} - \frac{4}{3h^2} F_{21}^{21},$$

$$b_5 = D_{11}^{22} - \frac{4}{3h^2} F_{11}^{22} + D_{21}^{21} - \frac{4}{3h^2} F_{21}^{21} - \delta_A\left(M_{11}^{22} - \frac{4}{3h^2} N_{11}^{22}\right),$$

$$b_6 = -R_{23}^{23} + \frac{4}{h^2} S_{23}^{23} = b_2,$$

$$b_8 = \delta_c\left(m_3 - \frac{4}{3h^2} m_5\right),$$

$$b_9 = -\delta_A\delta_B I_{33}^{22} - \delta_c \frac{4}{3h^2} m_5,$$

$$c_1 = R_{13}^{13} - \frac{4}{h^2} S_{13}^{13},$$

$$c_2 = R_{23}^{23} - \frac{4}{h^2} S_{23}^{23},$$

$$c_3 = R_{13}^{13} - \frac{4}{h^2} S_{13}^{13} + T_{11},$$

$$c_4 = R_{23}^{23} - \frac{4}{h^2} S_{23}^{23} + T_{22},$$

$$c_5 = 1 \ , \ c_6 = m_1 \ .$$

Here δ_A and δ_B are two tracers identifying the static and dynamic contributions of σ_{33}, respectively, whereas δ_c is a tracer identifying the effect of rotatory inertia terms (see [14,15]).

The coefficients of Eqs. (2) are:

$$a_1 = 0; \ a_2 = 0; \ a_3 = D_{11}^{11};$$

$$a_4 = D_{12}^{12}; \ a_5 = D_{22}^{11} + D_{12}^{12}; \ a_6 = - K^2 R_{13}^{13};$$

$$a_7 = - K^2 R_{13}^{13} \ ; \ a_8 = \delta_c m_3; \ a_9 = 0;$$

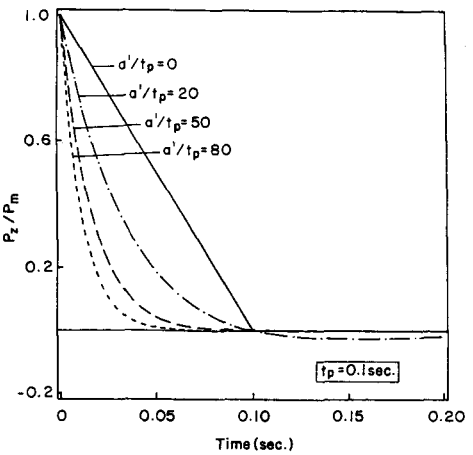

Fig. 1 Typical variation of blast overpressure with respect to time.

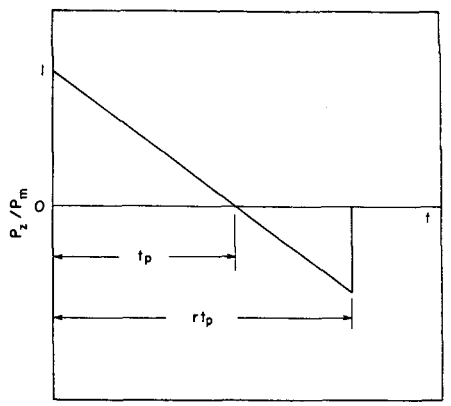

Fig. 2 Typical pressure time-history with an asymmetric N-shaped pulse.

$$b_1 = 0; \ b_2 = 0; \ b_3 = D_{22}^{22};$$

$$b_4 = D_{21}^{21}; \ b_5 = D_{11}^{22} + D_{21}^{21}; \ b_6 = - K^2 R_{23}^{23};$$

$$b_7 = - K^2 R_{23}^{23}; \ b_8 = \delta_c m_3; \ b_9 = 0;$$

$$c_1 = K^2 R_{13}^{13} \ ; \ c_2 = K^2 R_{23}^{23}; \ c_3 = K^2 R_{13}^{13} + T_{11};$$

$$c_4 = K^2 R_{23}^{23} + T_{22}; \ c_5 = 1; \text{ and } c_6 = m_1.$$

In the above expressions, D_{mn}^{ij}, F_{mn}^{ij}, ..., R_{mn}^{ij} denote the rigidity components and m_i ($i = 1,3,5$) are the reduced mass terms of the composite laminated plate defined in [17,18], while K^2 denotes a transverse shear correction factor.

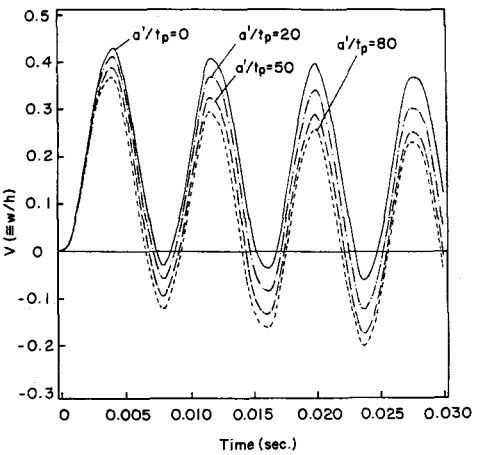

Fig. 3 Time history of the nondimensional deflection response of the center of a three-layered square plate (Structure A characterized by a/h = 15, a = 100 in. to a normal blast loading characterized by various a' and t_p = 0.1 s (the results are obtained within HSDT with p_m = 500 psi).

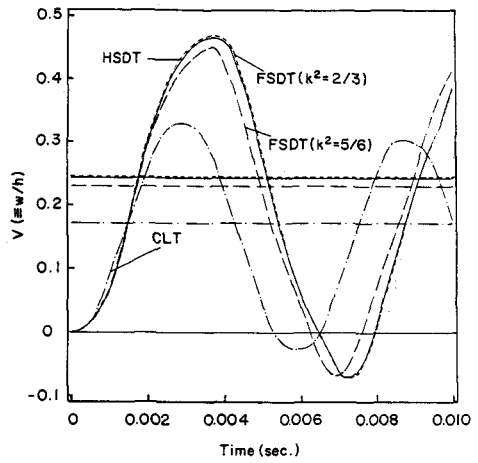

Fig. 4 Time history of the nondimensional deflection response of the center of a three-layered square plate (Structure B) (a/h = 20; a = 100 in.) to a blast loading characterized by t_p = 0.1 s, a' = 1.98 and p_m = 400 psi (the results are obtained within HSDT, FSDT, and CLT. The horizontal lines correspond to the static deflection, allowing one to emphasize the dynamic overshoot of the response).

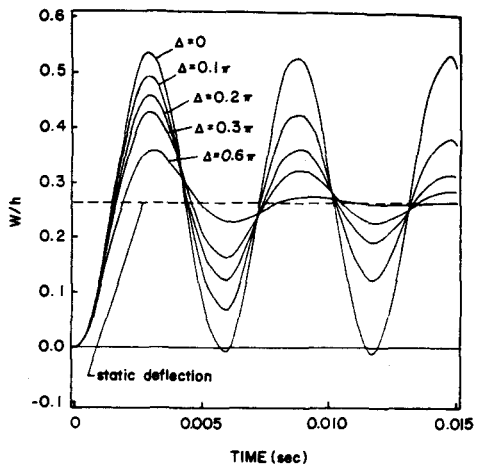

Fig. 5 Time-history of the nondimensional deflection of composite plates (Structure D) to a step pulse for five values of Δ/π = 0, 0.1, 0.2, 0.3 and 0.6. In addition, a = b = 60 in, a/h = 20; p_m = 250 psi.

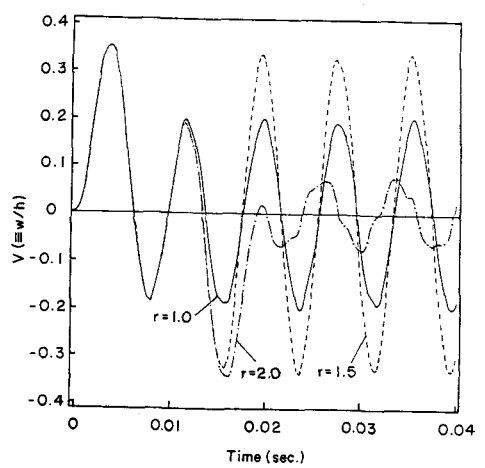

Fig. 6 Time history of the nondimensional deflection response of the center of a three-layered square plate (Structure A) (a/h = 15, a = 100 in.) to an N-shaped pulse characterized by various values of r and by P_m = 500 psi and t_p = 0.01 s (here HSDT was used only).

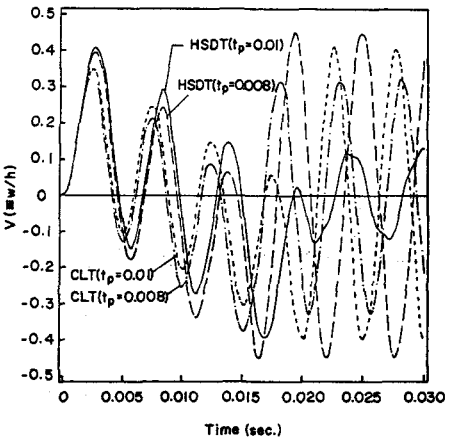

Fig. 7 Time history of the nondimensional deflection response of the center of a three-layered square plate (Structure A) (a/h = 10, a = 100 in.) subjected to a symmetric N-pulse characterized by two values of t_p and P_m = 2500 psi. Here the results are obtained within the framework of HSDT and CLT.

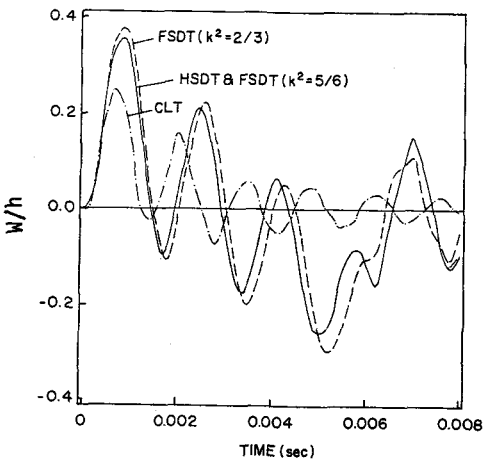

Fig. 8 *Time-history of the nondimensional deflection of composite* plates (Structure D) to an N-pressure pulse (r = 2), determined within HSDT and FSDT (with K^2 = 2/3 and k^2 = 5/6). In addition, a = b = 30 in; a/h = 10; Δ/π = 0.05; t_p = 0.003 sec; p_m = 2500 psi.

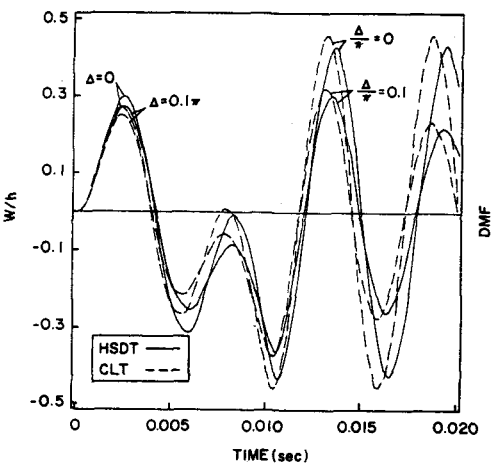

Fig. 9 Time-history of the nondimensional deflection of composite plates (Structure D) to an asymmetric N-pressure pulse (r = 2.5), determined within HSDT and CLT and for Δ/π = 0 and 0.1. In addition, a = b = 60 in; a/h = 20; t_p = 0.004 sec and p_m = 200 psi.

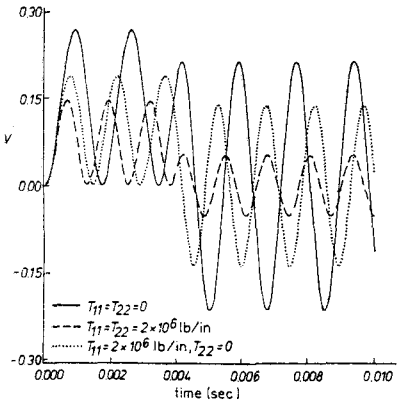

Fig. 10 The effect of in-plane edge loads on the center deflection response of an orthotropic plate to a step pulse ($\delta_A = \delta_C = \delta_B = 1$) (see [12], Fig. 3).

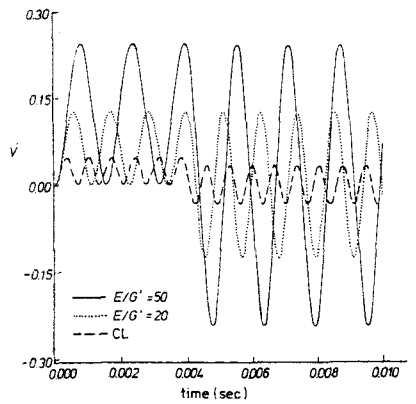

Fig. 11 Center deflection response of a transversely-isotropic plate of various E/G' ratios to a step pulse (see [12], Fig. 5).

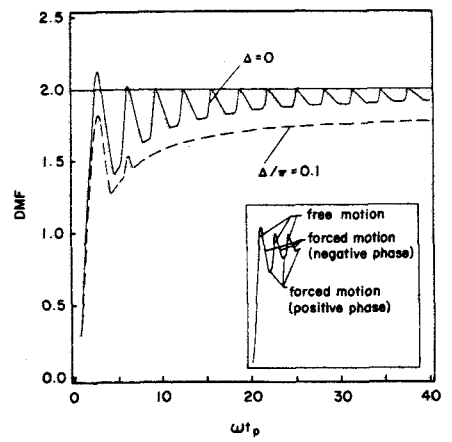

Fig. 12 Dynamic magnification factor variation vs. ωt_p of Structure D to an N-shaped pulse (r = 2) determined within HSDT for Δ/π = 0 and 0.1. In addition, a = b = 60 in; a/h = 20; p_m = 350 psi.

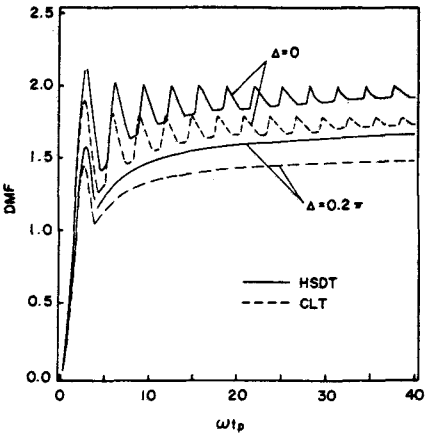

Fig. 13 Dynamic magnification factor variation vs. ωt_p of Structure D to an N-shaped pressure pulse ($r \geq 2$) determined within HSDT and CLT and for Δ/π = 0; 0.2. In addition, a = b = 60 in; a/h = 20.

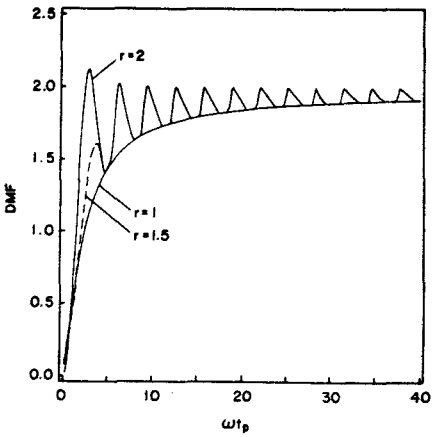

Fig. 14 Dynamic magnification factor variation vs. ωt_p of Structure D to an N-shaped pulse characterized by $r \geq 1$, 1.5, and 2. In addition, a = b = 60 in; a/h = 20; Δ/π = 0.